Letter

Probing the local density of states near the diffraction limit using nanowaveguide-collected cathode luminescence

Yoshinori Uemura, Masaru Irita, Yoshikazu Homma, and Mark Sadgrove*

Department of Physics, Faculty of Science, Tokyo University of Science, 1-3 Kagurazaka, Shinjuku-ku, Tokyo 162-8601, Japan

(Received 11 June 2021; accepted 18 August 2021; published 10 September 2021)

The photonic local density of states (PLDOS) determines the light-matter interaction strength in nanophotonic devices. For standard dielectric devices, the PLDOS is fundamentally limited by diffraction, but its precise dependence on the size parameter s of a device can be nontrivial. Here, we measure the PLDOS dependence on the size parameter in a waveguide using direct detection of cathode luminescence (CL) through the modes of a nanowaveguide. We observe that, depending on the position within the waveguide cross section, the effective diffraction limit of the PLDOS varies and the PLDOS peak shape changes. Our results are of fundamental importance for optimizing coupling to nanophotonic devices and also opening avenues for applications based on evanescently coupled CL photons.

DOI: 10.1103/PhysRevA.104.L031504

Introduction. The rate of decay of an emitter into a given optical mode is governed by Fermi's golden rule, and is proportional to the photonic local density of states (PLDOS) ρ associated with that mode. A fundamental limit on ρ for nanophotonic devices is the diffraction limit, which places a lower bound on the mode size of approximately half a wavelength along a given dimension [1]. Nonmetallic dielectric devices with a characteristic size less than this have suboptimal PLDOS due to redistribution of mode amplitude into the evanescent region—i.e., a loss of mode confinement. An operational definition of the diffraction limit for nanodevices is, therefore, the size at which the PLDOS is maximized.

An important class of diffraction limited nanodevices is that of nanowaveguides, which are used in fields ranging from quantum optics [2] and optomechanics [3] through to particle manipulation [4]. For certain nanowaveguide types, systematic measurement of the photonic local density of states via cathode luminescence (CL) spectroscopy [5–7] has been achieved via leaky modes. In this remarkable technique, depicted in Fig. 1(a), electrons incident on a device induce luminescence, offering essentially tomographic PLDOS reconstruction due to the point-dipole-like excitation provided by the electron beam [8–10]. However, because luminescence is collected in the far field, the PLDOS of true waveguide modes (which by definition do not couple to radiation modes) cannot be measured in general. Furthermore, although, it is well known from theoretical studies that an optimal diameter exists for coupling to nanowaveguides [11], experimental verification requires measurement of coupled luminescence from an arbitrarily located point dipole source through the waveguide modes, preferably with mode selection before detection. This is something which typical CL experiments are not suited to.

Here, we detect CL emitted into the fundamental mode of a nanowaveguide (optical fiber taper) *through the waveguide mode itself* as depicted in Fig. 1(b). We use this technique to characterize hitherto unmeasured aspects of the waveguide mode PLDOS. In particular, we measure the PLDOS dependence on the waveguide size parameter s (defined below) around the diffraction limit. Using different electron energies, we probe the PLDOS (i) close to the waveguide surface, where the near-field character of the mode is strong, and (ii) nearer to the waveguide center where the mode has a standard transverse wave character. These two regimes are shown to exhibit different dependence on the size parameter, and in particular a different effective diffraction limit. These results shed light on a fundamental characteristic of nanowaveguides and illuminate the subtle nature of the widely used diffraction limit concept for nanophotonic devices. Furthermore, the method of waveguide-coupled CL promises a way to create fiber coupled electrically driven photon sources and probe previously inaccessible characteristics of optical near fields using the CL technique.

Principle and methods. The principle of our experiment is shown in Figs. 1(b) and 1(c). Electrons from a scanning electron microscope (SEM) [12] penetrate a vacuum clad silica fiber (core refractive index $n_{\rm co} = 1.46$) of radius a ($200\ \text{nm} \leqslant 2a \leqslant 1\ \mu\text{m}$) to a depth δ, which depends on the electron energy. The fiber is tapered using a standard heat and pull technique [13]. We evaluated the SEM resolution to be about 5 nm [14,15], as explained in the Supplemental Material [16]. The electrons induce luminescence in the silica, a portion of which couples directly to the fiber fundamental modes with an intensity that depends on the photonic local density of states of the modes. As shown in Fig. 1(c), for a given value of δ and a position y along the fiber cross section, the radial position r and angle θ of the electron stopping position can be defined, with $\phi = \sin^{-1}(y/a)$, $r = \sqrt{y^2 + (a\cos\phi - \delta)^2}$, and $\theta = \pi/2 - \cos^{-1}(y/r)$. In Fig. 1(d), the so-parametrized stopping point of the electrons as a function of y is overlaid

*mark.sadgrove@rs.tus.ac.jp

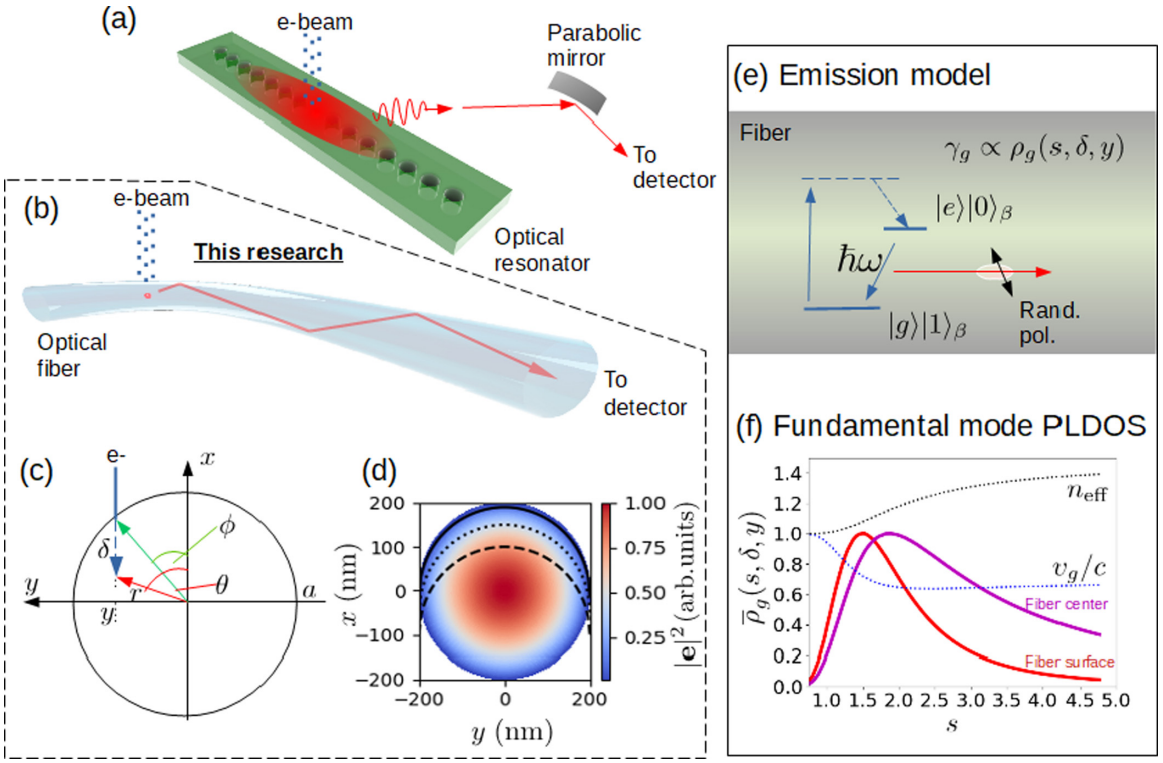

FIG. 1. Principle of the experiment. (a) Example of a standard cathode luminescence spectroscopy experiment. A resonant mode leaks photons which reach a detector in the far field. (b) Concept of the present work. Electrons are incident on a vacuum clad optical fiber of radius a and CL is detected through the guided mode itself. (c) Electrons incident at a point (a, ϕ) penetrate a distance δ into the fiber to point (r, θ) and induce cathode luminescence which couples directly to the fiber fundamental mode. (d) Intensity $|\mathbf{e}|^2$ of a circularly polarized fundamental (HE_{11}) mode of the fiber with curves showing an electron stopping position for $\delta = 10$ nm (solid line), $\delta = 50$ nm (dotted line), and $\delta = 100$ nm (dashed line). (e) Emission model. The energetic electron is assumed to excite an emitter within the fiber silica matrix to a high-energy level which then decays by nonradiative processes before emitting a randomly polarized photon into the fiber fundamental mode with propagation constant β at a center wavelength near 659 nm. (f) The thick red (magenta) line shows the normalized photonic local density of states $\bar{\rho}_g$ at the fiber surface (center) nm as a function of the size parameter s. Also shown are v_g/c (dotted blue line), and the effective refractive index of the mode $n_{\rm eff}$ (dotted black line)

on the profile of a fundamental fiber mode for the case where $a = 200$ nm, and the CL wavelength is 659 nm for three different values of δ.

As shown in Fig. 1(e), we assume that the measured light is from incoherent CL [5], which is produced in an effective off-resonant excitation process in which unpaired oxygen defect centers in the silica [17] are excited to a high energy level which decays nonradiatively before a final radiative transition produces randomly polarized luminescence with a phonon-broadened spectrum. The emission is assumed to occur at the point in the material where the electron comes to a stop, i.e., a distance δ from the fiber surface. We treat broadening of the excitation region phenomenologically by treating the electron beam as having a Gaussian distribution of a width similar to the penetration depth and convolving this distribution with the PLDOS.

Assuming a single mode fiber, the coupled intensity of the CL is proportional to the decay rate γ_g into the fundamental fiber modes at the position $\mathbf{r}_0$ in the fiber where CL is generated. In general we may write this relation as [1,18] $\gamma_g = \frac{2\mu_0\omega_0^2}{\hbar}\mathrm{Im}[\mathbf{p}\cdot\mathbf{G}_T(\mathbf{r}_0,\mathbf{r}_0,\omega_0)\cdot\mathbf{p}]$, where ω_0 is the transition resonant frequency, $\mathbf{p}$ is the dipole moment, and $\mathbf{G}_T$ is the guided mode transverse Green tensor. The imaginary part of the Green tensor may be evaluated [18,19] yielding $\mathrm{Im}[\mathbf{G}^T(\mathbf{r}_0,\mathbf{r}_0,\omega_0)] = \frac{c^2\mathbf{e}(\mathbf{r}_0)\mathbf{e}^*(\mathbf{r}_0)}{4v_g\omega_0}$. Here, v_g is the mode group velocity and $\mathbf{e}(\mathbf{r}_0)$ is taken to be the normalized mode function of the positive propagating, left-hand circular polarized HE_{11} fundamental mode of the fiber. The mode function is normalized according to the condition $1 = \int d^2r\, n(r)^2|\mathbf{e}(\mathbf{r_0})|^2$, where the integral is taken over a plane perpendicular to the fiber axis. The product of mode functions is interpreted as a dyad. Details of the mode functions are given in the Supplemental Material [16] and may be found in a number of places [11,20–22]. In our present study, the wavelength of the modes is fixed at $\lambda = 659$ nm, and the value that the mode function takes depends on the fiber radius a, at the radial position $\mathbf{r}_0(y,\delta)$. Note that the quantity $|\mathbf{e}(\mathbf{r}_0)|^2$ has units m^{-2} and may be considered to be a dimensionless-energy flux. This should be compared to the usual energy density associated with three dimensionally confined resonant modes.

Because Maxwell's equations are scale free, the functional dependence of the local density of states on the waveguide transverse dimension a or the wavelength λ is most generally expressed using the dimensionless size parameter $s = ka = (c/\omega_0)a$, where $k = 2\pi/\lambda$. By using a tapered fiber, we allow

the measurement of the PLDOS as a function of s for fixed λ and variable a.

By circular symmetry, a randomly polarized dipole couples with the same strength to either of the two orthogonally polarized fundamental modes. We may average over dipole polarization to produce the photonic local density of states associated with the fundamental modes [1]

$$\rho_g(s,\mathbf{r}) = \frac{2}{3}\frac{6\omega_0}{\pi c^2}\mathrm{Im}\{\mathrm{Tr}[\mathbf{G}(\mathbf{r}_0,\mathbf{r}_0,\omega_0)]\} = \frac{|\mathbf{e}(s,\mathbf{r}_0)|^2}{v_g}, \quad (1)$$

where the factor of $1/3$ arises from the average over dipole orientations and the factor of 2 arises due to the two possible orthogonal polarizations of the fundamental mode.

Finally, we see that

$$\overline{\gamma}_g = \frac{\pi\omega_0}{3\hbar\epsilon_0}p^2\rho_g(s,\mathbf{r}), \quad (2)$$

where $\overline{\gamma}_g$ is the decay rate into the fundamental modes averaged over polarization and the dipole moment strength is assumed to be $p = |\mathbf{p}|$ in any direction. Note that, for a given s, ρ_g contains all the dependence of $\overline{\gamma}_g$ on the fiber mode behavior. Our experimental measurements are of photon count rates through the fiber over some time Δt. It may be seen that such measurements are proportional to $\overline{\gamma}_g\Delta t \propto \rho_g$. In practice, we normalize both our measurements and the theoretical predictions for ρ_g so that their maxima are equal to unity before comparing them. We denote the so-normalized value of the PLDOS by $\overline{\rho}_g$.

The thick red line in Fig. 1(f) shows the normalized local density of states as a function of s just inside the fiber surface. The thick magenta line shows the same calculation made at the fiber center. Also shown are the scaled group velocity of the fundamental mode v_g/c (dotted blue line) and the effective refractive index n_{eff} for the fundamental mode (dotted black line). It may be seen that the peak region of the PLDOS is associated with the transition of v_g from the bulk silica value of $v_g \approx c/1.45$ to $v_g \approx c$ as the fiber mode is dominated by its evanescent component. Note that the maximum value of the unscaled PLDOS at the fiber center is almost three times larger than that just inside the fiber surface. Because the present experiment does not allow us to cleanly measure the relative amplitude of the PLDOS at these two different radial positions, we use the normalized PLDOS and focus on the differences seen in the peak position and peak width.

The most notable aspect of the PLDOS curves for different radial positions is that the peak value occurs at a different value of s. In this sense, the effective diffraction limit of s is different depending on where in the fiber cross section it is measured. This is a generic feature of waveguides (i.e., not just fibers) and occurs due to the behavior of the mode function $|\mathbf{e}(\mathbf{r})| = A(s)F(s,r)$, where $A(s)$ is a normalization factor depending only on the size parameter and $F(s,r)$ is in general a decreasing function of the radial distance r from the fiber center. Broadly speaking, $A(s)$ sets the intensity scale at a given value of s for a fixed optical power and thus has a peaked structure which gives rise to the diffraction limit. $F(s,r)$ can generally be written in the form $F(ur/a)$, where $u = a\sqrt{n_{\mathrm{co}}^2k^2 - \beta^2}$ is a dimensionless wave number which increases monotonically with the waveguide size parameter s. As r/a increases, the falloff in F as a function of u becomes steeper, leading to the peak of the PLDOS occurring at lower s. This is also the reason for the the narrower width of the PLDOS peak when $r = a$ compared with $r = 0$. More details are given in the Supplemental Material [16].

Experimentally, we detect the intensity in the fiber modes by passing a single mode fiber which is adiabatically connected to the fiber taper out of the SEM vacuum via a feedthrough [23]. The fiber can be connected to a spectrum analyzer or a modified Hanbury-Brown-Twiss setup which allows measurement of both polarization and the intensity correlation function $g^{(2)}$. In experiments, we used electron energies of 0.5 keV and 2 keV in a spot excitation configuration and 2 keV in a sweep excitation configuration. CL emitted into the fiber taper passed through a 630 nm cutoff single mode fiber to ensure that only light in the fundamental modes was collected. Further details of the experiment are given in the Supplemental Material [16].

Results. We now turn to our experimental results. First, we look at general properties of the fiber coupled cathode luminescence. The CL spectrum measured through the guided modes is shown in Fig. 2(a). A Lorentzian curve was fitted to the data and, as indicated, the center wavelength was found to be 659 nm and the full width at half maximum (FWHM) was found to be 56 nm. This spectrum is similar to that seen in silica fibers due to radiation induced defects or the fiber drawing process itself [17]. The luminescence has been attributed to unpaired oxygen atoms in the silica matrix.

We also checked the polarization at the fiber output by rotating both a half waveplate and a quarter waveplate before the light entered a polarizing beam splitter and measuring the output at both ports. For both waveplates, we saw variations in intensity of about $\pm 5\%$ of the mean value, suggesting nearly perfect random polarization.

Because little is known about the density of defects in silica which produce the observed cathode luminescence, we also measured the count coincidence rate of the CL through the guided modes. The normalized coincidence signal corresponds to the second-order correlation function $g^{(2)}(\tau) = \langle n(t)n(t+\tau)\rangle/[\langle n(t)\rangle\langle n(t+\tau)\rangle]$, where n denotes photon counts, the coincidence delay is given by τ, and $\langle\cdot\rangle$ denotes a time average. For a single or few emitters, an antibunching dip in the coincidence rate is expected at $\tau = 0$. As seen in Fig. 2(b), the measured correlation function shows no sign of antibunching and is consistent with a relatively large number of independent photon emitters within the excitation volume.

Next, we consider scans made of the fiber over its cross section for fiber diameters between 200 and 1000 nm. Figure 3(a) shows raw count rates (discrete points) joined by lines to guide the eye. It is notable that a large peak is observed at $2a = 400$ nm relative to the other diameters. This is due to the increased mode confinement at this diameter. Figure 3(b) shows the same experimental results normalized to allow easier comparison. In each case, curves showing values of $\overline{\rho}_g(a,\delta,y)$ for $\delta = 10$ nm convolved with a Gaussian profile with a standard deviation of 10 nm to account for the broad electron cascade process inside the silica. For these curves, we fitted the value of the amplitude and center position to the data. The fiber diameter was set to its experimentally measured value in the theory. Note that the colors of the points and curves correspond to the data shown in the same color

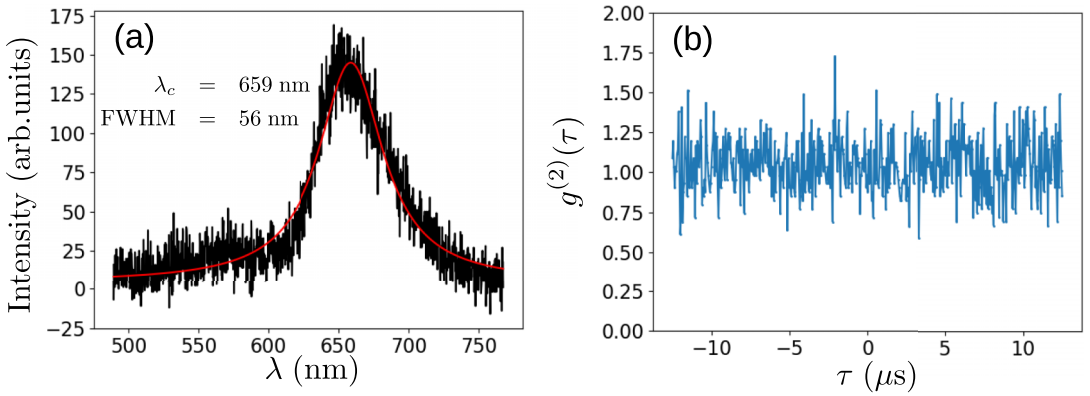

FIG. 2. (a) Measured spectrum of the fiber coupled CL. (b) Measured second-order correlation function $g^{(2)}(\tau)$ for a time difference τ between detection events.

in Fig. 3(a). Error bars show ± 1 standard deviation over ten intensity measurements.

The data show that the CL intensity varies only slowly across the fiber cross section. This is expected considering the circular symmetry of the coupling, i.e., a randomly polarized emitter should couple with the same strength to the fundamental modes at any position within the fiber that is a constant radial distance from its center. However, due to the stopping position on the x axis being dependent on y, the distance from the fiber center at which CL occurs changes, with the change becoming larger as the penetration depth increases.

Finally, we measured the waveguide coupled CL at different diameters using beam spot illumination at 0.5 keV ($\delta \approx 10$ nm [24]) and 2 keV ($\delta \approx 175$ nm [24]) positioned at the fiber center ($y = 0$). Results of these measurements are shown in Fig. 4. The PLDOS curve is calculated at $y = 0$ for the respective values of δ given above. The experimental results show generally good qualitative and quantitative agreement with the calculated PLDOS curve. In particular, the difference in the PLDOS peak position and the difference in the peak widths is clearly reproduced by the data. For the 0.5 keV data, we observe a peak at $s = 1.4$, whereas for 2.0 keV the peak occurs at $s = 1.9$. This corresponds to a difference in radius of 100 nm.

Discussion. In this work, we formulated the PLDOS for the fundamental mode of an optical fiber and experimentally evalutated the PLDOS by measuring CL coupled directly to the fiber fundamental modes. Using this technique, we made complete measurements of the PLDOS dependence on the size parameter around the diffraction limit. We clearly demonstrated the different PLDOS behavior for points near the fiber surface and nearer to the fiber center. Although previous CL measurements of photonic crystal waveguide modes do exist, they have relied on intrinsic losses or leaky modes which coupled to the far field [7]. Likewise, although the coupling efficiency from point emitters to the modes of a fiber has been

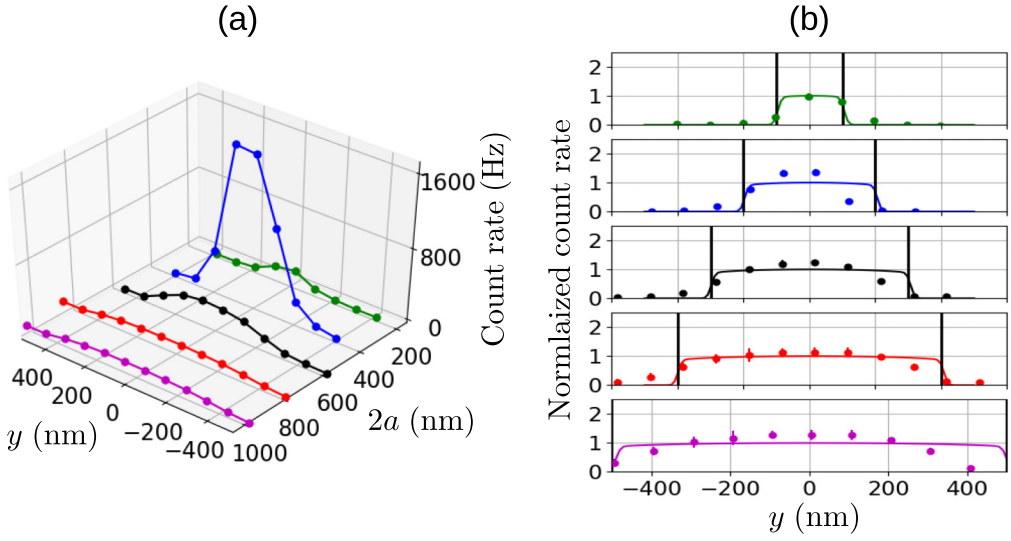

FIG. 3. Spot scans perpendicular to the optical fiber axis for electron energies of 0.5 keV. (a) Unnormalized data (discrete points) for five different fiber diameters with lines connecting points to guide the eye. (b) The same data normalized and fitted by $\overline{\rho}_g(a, \delta, y)$ convolved with a Gaussian beam profile. From top to bottom, the data shown is for $2a = 200$, 400, 600, 800, and 1000 nm. Theoretical curves for $\delta = 10$ nm are shown for each case

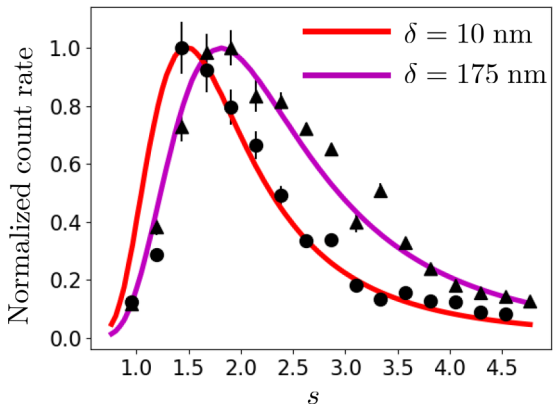

FIG. 4. Measurement of relative PLDOS as a function of diameter. Circles show measurements made using a stationary electron beam of energy 0.5 keV at the fiber center. The measurements shown are the averaged raw data, with error bars showing the standard deviation over ten separate measurements. The red curve shows $\overline{\rho}_g(a, \delta = 10\ \text{nm}, y = 0)$. Triangles show similar measurements, but for a beam energy of 2.0 keV, which corresponds to $\delta = 175$ nm. The theoretical value of $\overline{\rho}$ in this case is shown by the magenta curve.

measured, these measurements suffered from large systematic errors and did not reveal the full behavior of the PLDOS itself [25]. In contrast we are able to clearly measure the difference in PLDOS behavior near the fiber surface and nearer to the fiber center even though the respective PLDOS peak positions differ by a fiber radius of just 100 nm.

This work successfully enlarges the domain in which CL spectroscopy may be applied, from its original application to modes with a radiative component to the case of completely bound photonic states of which the modes of a waveguide are one example. Although for any finite waveguide, the concept of a bound state is approximate, the one meter length of the waveguide used here is several orders of magnitude larger than that of waveguides previously explored with the CL technique, making the bound state (i.e., guided mode) assumption reasonable. It should also be possible to use our technique to couple electron beam induced luminescence from more general nonradiative modes which do not couple to the far field. Such modes can couple via the evanescent field of the optical fiber taper to its guided modes and thus be detected as in the present experiment, opening up CL spectroscopy to regimes which could traditionally only be measured using electron energy loss (EEL) methods.

One possible objection to the above is that a similar effect can be achieved by capturing the light output from the end of the fiber using a standard free space collection configuration [e.g., as depicted in Fig. 1(a)]. However, this does not preserve mode information, which is important because different waveguide modes have different evanescent field characteristics. In the present experiment, for example, we were able to measure only the fundamental mode by splicing a single mode fiber to the output of the tapered fiber. In principle, information about higher-order modes could also be extracted by using few-mode fibers as mode filters.

In terms of applications typical fiber coupled photon sources up to now have used optically excited emitters [25–27]. Our method should provide a route to achieving waveguide-coupled, electrically driven photon sources [28–30], and allow a more deterministic approach even for nondeterministically assembled composite nanodevices created by combining nanowaveguides with colloidal nanocrystals.

For the above reasons, we believe that the technique detailed here can open opportunities to study fundamental aspects of nanooptics by measuring PLDOS through nanowaveguide modes, while also providing a platform for applications.

Acknowledgments. M.S. thanks F. Le Kien for valuable discussions regarding the photonic local density of states. This work was supported by the Nano-Quantum Information Research Division of Tokyo University of Science. Part of this work was supported by JST CREST (Grant No. JPMJCR18I5).

[1] L. Novotny and B. Hecht, *Principles of Nano-optics* (Cambridge University Press, Cambridge, UK, 2012).
[2] I. Aharonovich, D. Englund, and M. Toth, Nat. Photon. **10**, 631 (2016).
[3] B. Khanaliloo, H. Jayakumar, A. C. Hryciw, D. P. Lake, H. Kaviani, and P. E. Barclay, Phys. Rev. X **5**, 041051 (2015).
[4] A. H. Yang, S. D. Moore, B. S. Schmidt, M. Klug, M. Lipson, and D. Erickson, Nature (London) **457**, 71 (2009).
[5] F. J. Garcia de Abajo, Rev. Mod. Phys. **82**, 209 (2010).
[6] A. Polman, M. Kociak, and F. J. G. de Abajo, Nat. Mater. **18**, 1158 (2019).
[7] B. J. Brenny, D. M. Beggs, R. E. van der Wel, L. Kuipers, and A. Polman, ACS Photon. **3**, 2112 (2016).
[8] A. C. Atre, B. J. Brenny, T. Coenen, A. García-Etxarri, A. Polman, and J. A. Dionne, Nat. Nanotechnol. **10**, 429 (2015).
[9] R. Sapienza, T. Coenen, J. Renger, M. Kuttge, N. Van Hulst, and A. Polman, Nat. Mater. **11**, 781 (2012).
[10] A. Hörl, G. Haberfehlner, A. Trügler, F.-P. Schmidt, U. Hohenester, and G. Kothleitner, Nat. Commun. **8**, 37 (2017).
[11] F. Le Kien, S. Dutta Gupta, V. I. Balykin, and K. Hakuta, Phys. Rev. A **72**, 032509 (2005).
[12] H. Jaksch and J. Martin, Fresenius' J. Anal. Chem. **353**, 378 (1995).
[13] J. M. Ward, D. G. O'Shea, B. J. Shortt, M. J. Morrissey, K. Deasy, and S. G. Nic Chormaic, Rev. Sci. Instrum. **77**, 083105 (2006).
[14] M. Irita, S. Yamazaki, H. Nakahara, and Y. Saito, IOP Conf. Ser.: Mater. Sci. Eng. **304**, 012006 (2018).
[15] M. Irita, H. Nakahara, and Y. Saito, e-J. Surf. Sci. Nanotechnol. **16**, 84 (2018).

[16] See Supplemental Material at http://link.aps.org/supplemental/10.1103/PhysRevA.104.L031504 for information regarding fiber mode functions and details of the experiment.
[17] G. Sigel, Jr. and M. Marrone, J. Non-Cryst. Solids **45**, 235 (1981).
[18] T. Søndergaard and B. Tromborg, Phys. Rev. A **64**, 033812 (2001).
[19] F. Le Kien, D. Kornovan, S. S. S. Hejazi, V. G. Truong, M. Petrov, S. N. Chormaic, and T. Busch, New J. Phys. **20**, 093031 (2018).
[20] K. Okamoto, *Fundamentals of Optical Waveguides* (Academic Press, New York, 2006).
[21] F. Le Kien, J. Liang, K. Hakuta, and V. Balykin, Opt. Commun. **242**, 445 (2004).
[22] F. Le Kien, T. Busch, V. G. Truong, and S. N. Chormaic, Phys. Rev. A **96**, 023835 (2017).
[23] E. R. Abraham and E. A. Cornell, Appl. Opt. **37**, 1762 (1998).
[24] B. Raftari, N. Budko, and K. Vuik, AIP Adv. **8**, 015307 (2018).
[25] R. Yalla, F. Le Kien, M. Morinaga, and K. Hakuta, Phys. Rev. Lett. **109**, 063602 (2012).
[26] M. Fujiwara, K. Toubaru, T. Noda, H.-Q. Zhao, and S. Takeuchi, Nano Lett. **11**, 4362 (2011).
[27] R. Yalla, M. Sadgrove, K. P. Nayak, and K. Hakuta, Phys. Rev. Lett. **113**, 143601 (2014).
[28] E. Le Moal, S. Marguet, B. Rogez, S. Mukherjee, P. Dos Santos, E. Boer-Duchemin, G. Comtet, and G. Dujardin, Nano Lett. **13**, 4198 (2013).
[29] L. H. G. Tizei and M. Kociak, Phys. Rev. Lett. **110**, 153604 (2013).
[30] S. Meuret, L. H. G. Tizei, T. Cazimajou, R. Bourrellier, H. C. Chang, F. Treussart, and M. Kociak, Phys. Rev. Lett. **114**, 197401 (2015).